Coupling strongly correlated electron systems to a tunable electronic reservoir

S. Bag [1,3] L. Fratino [1] A. Camjayi,[2] M. Civelli,[1] and M. Rozenberg [1]
[1]*Université Paris-Saclay, CNRS Laboratoire de Physique des Solides, 91405 Orsay, France*
[2]*Universidad de Buenos Aires, Ciclo Básico Común and CONICET - Universidad de Buenos Aires, Instituto de Física de Buenos Aires (IFIBA), Buenos Aires 1428, Argentina*
[3]*Department of Physics, Arizona State University, Tempe, Arizona 85287, USA*

(Received 27 October 2023; revised 27 January 2024; accepted 6 May 2024; published 31 May 2024)

We study the effect of coupling an electronic reservoir to a Hubbard model and to a dimer Hubbard model. This is motivated by recent experiments on the effect of illumination on the insulator-metal transition in a vanadium oxides and photoconductive cadmium sulfide heterostructure. We model the system as an electronic reservoir hybridized to the correlated system. We assume that the light intensity controls the hybridization coupling strength. We find that the light intensity acts similarly as the temperature in the weak interaction regime. This is consistent with the role played by electronic reservoirs in out-of-equilibrium systems. In contrast, qualitative differences appear at strong coupling. We show that modeling the V_2O_3 compound with a Hubbard model, our results describe qualitatively well the observed illumination-driven suppression of the insulator-metal transition. In contrast, in the DHM results fail to capture the mild suppression observed in the case of VO_2. This indicates that the lattice may play an important role in this case.

DOI: 10.1103/PhysRevB.109.195171

I. INTRODUCTION

Mott insulator materials are interesting for neuromorphic devices, such as artificial spiking neurons [1–3]. The several orders-of-magnitude changes of the resistivity across the metal-to-insulator-transition (MIT) of Mott insulators can be exploited in artificial neuromorphic devices to recreate the all-or-nothing excitation of an action potential [2–6]. Furthermore, there are several ways to control the Mott MIT, namely by changing doping, pressure, electric field, etc. [7–19]. A particularly interesting possibility, in the context of neuromorphic applications, is to control the transition by illumination with light in hybrid thin-film structures where one changes the coupling between the Mott material and its environment [17,20,21].

In recent years, the study of phenomena that emerge from the control of the coupling between a system to a reservoir is attracting significant attention. In experiments, changing the environment coupling can lead, for instance, to line-width broadening [22], decoherence, and a finite lifetime of states [23]. Moreover, it can allow tailoring desired states, like entangled [24], antiferromagnetically (AFM) ordered [25], Bose condensed [26], etc. While this has been so far considered mostly in the context of cold atoms, it is also potentially relevant for electronic properties of solid state systems, including strongly correlated ones. For instance, an important case is that of systems with metal-insulator transitions that are driven out of equilibrium. In those cases, it has been recognized that coupling to an electronic reservoir is an essential physical ingredient to achieve a steady state in a static electric field-driven Hubbard model (HM) [27–32]. Hence, it is an important question to consider the systematic effect that the coupling to an electronic reservoir may have on a given strongly correlated system.

In addition to the previous motivation, the effect of a (semi)metallic reservoir coupled to a strongly correlated system is also relevant for heterostructures. Indeed, the ability to grow multilayers including high quality strongly correlated oxides, prompted the interest in understanding the fate of the Mott metal-insulator transition in metal and semimetal/Mott-insulator hybrid systems [33].

For example, in the study of heterostructures of a metal/AFM-Mott model, a suppression of AFM structure factor is observed in the AFM-Mott layer due to its proximity to the metal [34,35]. However, it was also reported that the effect of an additional conduction band in the periodic Anderson model can lead to stabilization of the AF order [36–38] in the system. Furthermore, in the heterostructure of a paramagnetic (PM) metal and a PM-Mott insulator, the metal state may penetrate into the Mott insulator side [39–41].

A particularly interesting type of Mott insulator materials are the vanadium oxides VO_2 and V_2O_3, which have temperature-driven MITs [42].

In a recent experiment, the effects on the MIT was studied in the heterostructure of vanadium oxide and the photoconductive semiconductor cadmium sulfide (CdS), for various levels of illumination [17]. Interestingly, both VO_2 and V_2O_3 showed a suppression of MIT with the power of light illuminated on CdS. However, the modulation of the MITs in VO_2 and V_2O_3 were dramatically different. The illumination quickly suppressed the T_{MIT} of V_2O_3, driving it down toward zero temperature. While it only had a minor suppression effect on T_{MIT} of VO_2, shifting it down by just a few degrees.

The present study is motivated by those experiments. We aim to understand the suppression of T_{MIT} in vanadium oxides/CdS heterostructures in the presence of light. To that goal, we need to model both the effect of the CdS and also the MITs in V_2O_3 and VO_2. In the case of V_2O_3, the MIT

occurs between an AFM insulator to a PM metallic state. In this initial study, for the sake of simplicity, we shall follow the recent study [43] to model the transition. In that paper, it was shown that the single-band HM treated within DMFT was able to capture nontrivial features of the T-driven MIT with AFM symmetry breaking at half-filling, such as the anomalous enhancement of the negative magnetoresistance. On the other hand, the MIT in the case of VO_2 is qualitatively different, since it is nonmagnetic. Moreover, the Mott insulator phase of VO_2 is monoclinic, where pairs of V atoms are dimerized, presumably forming "dynamical singlets" [44]. Fortunately, in this case we can also count on a simple model that captures basic nontrivial features of the MIT, which we can adopt in this initial study. This is the dimer Hubbard model (DHM), which is an extension of the Hubbard model where each unit cell contains a dimer. It was recently shown that the DMFT solution of the model exhibits a T-driven first-order nonmagnetic MIT at half-filling, where the ground state is a dimerized Mott insulator with dynamical singlets [45–48]. Hence, in this initial study we shall adopt these two simple models as zero-order approximation to describe the MITs of V_2O_3 and VO_2 in the presence of a tunable hybridization.

One of our main results is that the reservoir may qualitatively act as a temperature and can may suppress the T_{MIT} in agreement with the experimental observations on V_2O_3. However, the comparison with observations in VO_2 there seems to remain some significant quantitative differences. We shall argue later on that this may point to a relevant role played by the lattice degree of freedom that are not included in our model [49].

This paper is organized as follows: In Sec. II we describe the model and the numerical approaches. Then, in Sec. III we shall describe the results. Firstly, we discuss the systematic effect of T and Γ on the AFM phase and the MIT of the single-band HM. Secondly, we shall describe the effects of those parameters for the interaction-driven PM insulator-metal transition in both the HM and the DHM. While the former is not directly relevant to the physics of the vanadates, we find it useful to include that study as a reference case, since it is the most widely studied MIT within DMFT. In the last Sec. V, we discuss the comparison of our findings with experimental results, including the possible origin of some standing discrepancies.

II. MODELS AND METHOD

Our task is to model the hybridization effect of CdS, which is a good photoconductive semiconductor [50,51]. In dark it is highly insulating, i.e., more than the Mott insulator states in the vanadium oxides. However, when illuminated by light it creates a substantial amount of electron-hole pairs and, in consequence, shows a drop in the resistivity. Nevertheless, CdS never has truly metallic character but remains a semiconductor, i.e., does not have metallic conduction. Therefore, we propose to model the CdS as a set of electronic reservoirs that are locally coupled with the V sites. In other words, we consider that the excited electron-hole pairs are described as incoherent metallic states that locally hybridize with those of the vanadium oxides. Since the vanadate thin films are of the order of 10 nm, we shall also assume that the electric conduction is dominated by the physics of the interface, which we model as a layer of HM or DHM hybridized with electronic reservoirs at each lattice site. As increasing the light intensity on the CdS one can tune the number of (photo)carriers, we model this effect through the strength of the hybridization parameter $\Gamma = \gamma^2 \rho(E_F)$. γ is a geometrical parameter independent of the light intensity as it describes the hybridization hopping amplitude between the sites that represent the CdS and the vanadium oxide layers, respectively. On the other hand, $\rho(E_F)$ represents the density of states of the CdS, which increases with light intensity. However, the detailed dependence of $\rho(E_F)$ and the intensity of illumination, that is experimentally controlled by the power on the LED light, is not trivial. Therefore, here, for the sake of definiteness and simplicity, we assume that the control parameter Γ (through the effect of ρ) is proportional to the power of the LED.

Before going into the technical details of the model, we may consider one additional aspect about the validity of the description of CdS by an electronic bath. Unlike electrons in a metal, the carriers in CdS are in a steady state but out-of-equilibrium. This is because they are continuously created as particle-hole pairs and recombining. Since we shall be adopting DMFT as methodology, which maps the lattice models into associated Kondo-like quantum-impurity problems [52]. Hence, a valid question is whether those carrier will be able to provide "Kondo screening" to the quantum impurity. To address this issue we should consider the relevant timescales. The ordinary Kondo-screening time can be estimated from the inverse of the typical Kondo temperature, T_K 10 K, i.e., τ_K 10^{-12} sec. However, this is not the relevant timescale, because within DMFT the Kondo scale corresponds to the width of the metallic quasiparticle peak at the Fermi energy. Unless very close to a metal-insulator transition critical point where there may be substantial mass enhancements, this effective Fermi energy scale can be estimated as ϵ^* 0.1 eV. This value is appropriate for vanadates and corresponds to τ_{scr} 10^{-14} sec, i.e., a much shorter timescale than for the ordinary Kondo impurity screening. The timescale τ_{scr} should be compared to the recombination time τ_{rec} of the excited electron-hole pairs. One may naively expect that this time is set by the inverse of the semiconducting gap, which in the case of CdS is 2.4 eV, hence, τ_{rec} 10^{-15} sec. Therefore, $\tau_{rec} < \tau_{scr}$, so *a priori* the recombination would happen too fast to provide screening. However, this is not quite the case. The recombination time in CdS has been measured (see, for instance, [53]) with reported values of τ_{rec} 10^{-9} sec, i.e., much longer than the naive estimate. In fact, the case is that $\tau_{rec} \gg \tau_{scr}$, which indicates that the approximation made in our model seems qualitatively safe.

A. Hubbard model (HM)

The Hamiltonian of the single-band HM coupled with an incoherent electronic reservoir reads as

$$\hat{\mathcal{H}} = -t \sum_{\langle i,j\rangle,\sigma} (\hat{c}^\dagger_{i\sigma}\hat{c}_{j\sigma} + \text{H.c}) + U \sum_i \hat{n}_{i\uparrow}\hat{n}_{i\downarrow} - \mu \sum_{i,\sigma} \hat{c}^\dagger_{i\sigma}\hat{c}_{i,\sigma} + \sum_{i,\sigma} \hat{\mathcal{H}}^{i\sigma}_c, \quad (1)$$

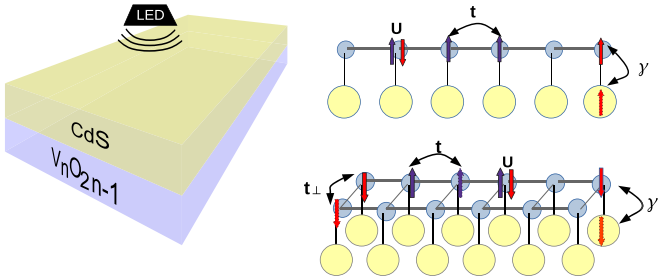

FIG. 1. Schematic experimental setup for CdS/V_nO_{2n-1} heterostructures with light on CdS where $n = 2$ corresponds to CdS/V_2O_3 and $n = \infty$ corresponds to CdS/VO_2. Schematic representation of HM (top right) and DHM (bottom right) with electronic reservoir connected to each site of the lattice. t is the hopping amplitude of an electron between nearest-neighbor sites. γ is the hopping amplitude of an electron between the site and the electronic reservoir. $t_\perp$ is the hopping amplitude of an electron between dimer sites.

where $\hat{c}^\dagger_{i\sigma}$ and $\hat{c}_{i\sigma}$ are respectively the fermionic creation and annihilation operators at the ith site of the lattice and $\hat{n}_{i\sigma} = \hat{c}^\dagger_{i\sigma}\hat{c}_{i\sigma}$ is the number operator. Here t is the hopping amplitude of an electron between nearest-neighbor sites, U is the on-site repulsion energy if two electrons (of opposite spins) occupy the site, and μ is the chemical potential of the system, controlling filling. We fixed μ at $U/2$ for the half-filled case. Last term of the Hamiltonian, $\sum_\sigma \hat{\mathcal{H}}^{i\sigma}_c$, represents the coupling of an electronic reservoir with ith site of the lattice. Details about this coupling term are given in the later part of this section. The top-left panel of Fig. 1 displays a schematic representation of HM with the electronic reservoir connected to each site of the lattice.

We solve this model using DMFT with a semicircular density of states, $D(\epsilon) = \frac{2}{\pi D^2}\sqrt{(D^2 - \epsilon^2)}$ with half band width $D = 1$. DMFT provides the exact solution of the model [43,52] on the Bethe lattice. We solve the impurity problem of DMFT using hybridization expansion-continuous-time quantum Monte Carlo (HYB-CTQMC) [54–56]. We solve the model both with and without AFM symmetry. We present the result of the HYB-CTQMC in Sec. III.

B. Dimer Hubbard model (DHM)

An interesting extension of single-band HM is the DHM [57]. This schematic model was shown to capture some key qualitative features of the temperature-driven MIT transition of VO_2 [45,46,48]. The DHM Hamiltonian, coupled with an incoherent electronic reservoir reads,

$$\begin{aligned}\hat{\mathcal{H}} = &-t\sum_{\langle i,j\rangle,\sigma,\alpha}(\hat{c}^\dagger_{i\alpha\sigma}\,\hat{c}_{j\alpha\sigma} + \text{H.c}) + \\ &+ t_\perp\sum_{i,\sigma}(\hat{c}^\dagger_{i1\sigma}\,\hat{c}_{i2\sigma} + \text{H.c.}) + \\ &+ U\sum_{i,\alpha}\hat{n}_{i\alpha\uparrow}\,\hat{n}_{i\alpha\downarrow} - \mu\sum_{i,\alpha,\sigma}\hat{n}_{i\alpha\sigma} + \sum_{i,\alpha,\sigma}\hat{\mathcal{H}}^{i\alpha\sigma}_c,\end{aligned} \tag{2}$$

where the index i and j denote the lattice cells, $\alpha = 1, 2$ denotes the dimer sites within a given cell and σ labels the spin. The hopping t and $t_\perp$ correspond to the amplitudes between nearest-neighbor lattice cells and between dimer sites, respectively. The last term of the Hamiltonian, $\sum_\sigma \hat{\mathcal{H}}^{i\sigma\alpha}_c$, represent the electronic reservoir coupled to ith lattice cell's dimer site α. Note that we use an independent electronic reservoir for each site of the dimer as can be seen in the schematic representation of the model in the bottom-right panel of Fig. 1. Details about the electronic reservoir are given later in this section. The local Green's function of the lattice becomes diagonal in the bond (B) and antibond (AB) basis, where the creation operator in the B and AB basis is related to the site basis by the following equation:

$$\hat{c}^\dagger_{iAB/B\sigma} = \frac{\hat{c}^\dagger_{i1\sigma} \pm \hat{c}^\dagger_{i2\sigma}}{\sqrt{2}}. \tag{3}$$

Therefore, we find it practical to solve the model on this basis.

C. Electronic reservoirs

The Hamiltonian of the electronic reservoir coupled to each lattice site of the models (HM or DHM) reads

$$\sum_\sigma \hat{\mathcal{H}}^{i\sigma}_c = \sum_{k,\sigma}\epsilon_k\hat{a}^\dagger_{ik\sigma}\hat{a}_{ik\sigma} + \gamma\sum_{l,\sigma}(\hat{a}^\dagger_{il\sigma}\hat{c}_{i\sigma} + \text{H.c.}) \tag{4}$$

where $\hat{c}_{i\sigma}$ denotes the fermionic operator at site i for the HM (or similarly, adding a label α, at the ith cell's α site for DHM) and $\hat{a}_{il\sigma}$ is the fermionic operator for reservoir's electron. ϵ_l are the reservoir's electron energy levels. For simplicity, we assume that the reservoir's electrons hybridize with the lattice fermions with constant amplitude γ. We can integrate out the noninteracting reservoir's electrons, and their effect appears as an additional effective hybridization for the c fermions at each impurity site, which remains fixed in the DMFT calculation. This effective hybridization due to the reservoir's electrons reads as

$$\Delta_\Gamma(\omega_n) = \sum_l \frac{\gamma^2}{i\omega_n - \epsilon_l} = \int d\epsilon\,\rho_l(\epsilon)\frac{\gamma^2}{i\omega_n - \epsilon}. \tag{5}$$

For simplicity, we adopt a semicircular density of states for the reservoir electrons, $\rho_l(\epsilon) = \frac{2}{\pi D'^2}\sqrt{(D'^2 - \epsilon^2)}$, so the above integration takes the closed form

$$\Delta_\Gamma(\omega_n) = -\frac{2D'i\Gamma}{\omega_n + sig(\omega_n)\sqrt{\omega_n^2 + D'^2}} \tag{6}$$

where $\Gamma = \gamma^2/D'$ controls the strength of the effect of hybridization with a reservoir. For convenience, we choose half the bandwidth of the electronic reservoir $D' = 1.0$.

D. Details on the DMFT method

We describe here how the hybridization of the associated impurity problem is modified by the presence of the reservoirs.

In the case of the HM we shall consider both solutions with and without AFM symmetry. The effect of the reservoir within DMFT is most clearly observed through the self-consistency condition of the associated quantum impurity problem [52]. The total hybridization function reads

$$\Delta_\sigma(\omega) = t^2 G_{\text{loc},\bar{\sigma}}(\omega) + \Delta_\Gamma(\omega) \tag{7}$$

where we observe that the reservoir is simply added to the quantum single-site environment. For further details on the DMFT method and self-consistent equations for the AFM-HM see Refs. [43,52].

In the case of the DHM, we consider the AB/B basis, hence the total hybridization entering the DMFT self-consistency equation becomes

$$\Delta_{AB/B\sigma}(\omega) = t^2 G_{\mathrm{loc},AB/B\sigma}(\omega) + \Delta_\Gamma(\omega). \tag{8}$$

For further details on the DMFT self-consistent equations for the DHM see Refs. [45,48,58].

As model parameters, we adopt in the case of the HM $t = 0.5$ (since we already set $D = 1$), and we fix on-site local repulsion $U = 1.7$, which was found adequate to describe the AFM-PM MIT in V_2O_3 [43]. For the DHM we also adopt $t = 0.5$, and then fix $t_\perp = 0.3$ and the on-site local repulsion $U = 2.2$, as where already shown to be adequate to qualitatively describe the PM MIT in VO_2 [45,48]. In addition, we shall also consider for both models and for the sake of obtaining a full qualitative picture of the behavior, a large value of $U = 4$. This sets the systems well into their Mott insulator states, so the MIT actually would become an "insulator-insulator" transition. However, as we shall see, the presence of the reservoirs will change this naif expectation.

The DMFT calculation with the HYB-CTQMC impurity solver produces data in Matsubara frequency. However, to obtain the behavior of the density of state (DOS) and the DC resistivity, one requires real-frequency data. Therefore, we use the maximum entropy method to get the analytical continued Green's function [56,59]. From the Green's function in real frequency, one can then calculate the local DOS [$\mathcal{A}(\omega)$], which reads

$$\mathcal{A}(\omega) = -\frac{1}{\pi} Im\, G(\omega^+). \tag{9}$$

For the HM we shall show the total DOS, i.e., the average of the two spin projections, $\mathcal{A}_{\mathrm{HM}}(\omega) = \frac{1}{2}\sum_\sigma \mathcal{A}_\sigma(\omega)$. Whereas, for the DHM, the total DOS results from the average of spin and B/AB-symmetry projections, $\mathcal{A}_{\mathrm{DHM}}(\omega) = \frac{1}{4}\sum_\sigma (\mathcal{A}_{B,\sigma}(\omega) + \mathcal{A}_{AB,\sigma}(\omega))$. Expressions for the conductivity of the HM and the DHM are given in the Appendices.

III. RESULTS AND DISCUSSION

A. Hubbard model with antiferromagnetic symmetry

We begin with the MIT in the single-band HM model case, which occurs in the presence of antiferromagnetism. In the absence of an electronic bath, the low-temperature state is an AFM insulator, and there is a U-dependent T_N where magnetization goes to zero, and the gap closes, and one has the T-driven MIT. The presence of an AFM state is signaled by the staggered magnetization ($m_s = |n_\uparrow - n_\downarrow|$) order parameter.

Figure 2 shows how m_s continuously goes to zero as a function of T for $U = 1.7$ and for $U = 4.0$, when Γ=0. Interestingly, similarly as the effect of T, we observe that Γ can also suppress the AFM ordering in HM at both low and high U, when T is fixed at a small value. One may be tempted to conclude that Γ behaves qualitatively as T. However, the systematic results shown in Fig. 3 shows otherwise. They display

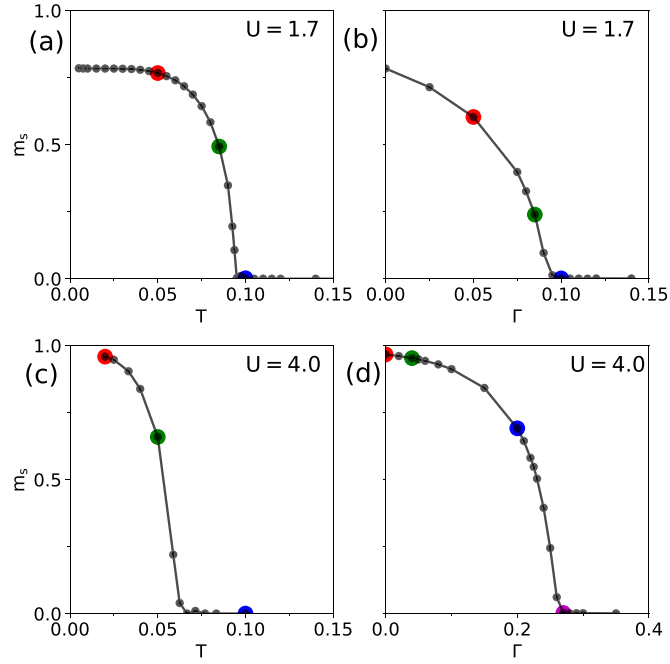

FIG. 2. [(a),(b)] The variation of the staggered magnetization as a function of T and Γ, respectively, for HM at $U = 1.7$; [(c),(d)] the same at $U = 4.0$. We observe that both thermal fluctuations and Γ can suppress the AFM order, seemingly playing a qualitatively similar role [$T = 0.01$ in (b) and (d)].

the variation of Néel's temperature (T_N) and, similarly the Γ_N that signals the critical Γ value that drives the magnetization to zero, as a function of U. The data reveals that the dependence is qualitatively different. In the absence of reservoirs, T_N has the well-known nonmonotonous dependence on U [52,60,61]. For small U, T_N increases with increasing U, as the AFM gap increases with both m_s and U. While at large U, T_N changes its behavior and decreases with increasing U, since the magnetic exchange coupling decreases as $\sim t^2/U$. For the case of Γ at low T we observe that for low values of interaction U, it seems to produce an effect similar to T, as was expected from the results of Fig. 2. However, in stark contrast, we observe that at larger values of U, the critical Γ_N increases monotonously

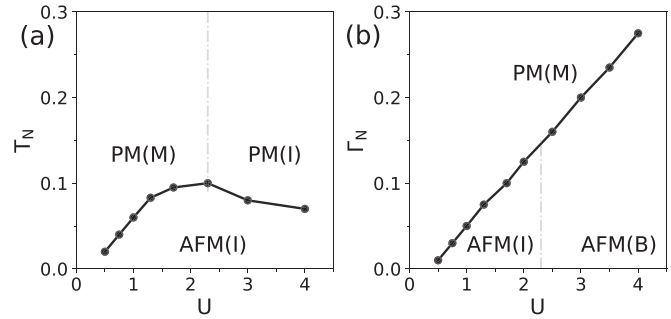

FIG. 3. (a) T-U phase diagram for $\Gamma = 0.0$ and (b) Γ-U phase diagram for $T = 0.01$ of the half-filled HM with AFM symmetry. M, I, and B label metal, insulator, and bad metal, respectively. Dashed lines approximately denote the phase boundaries.

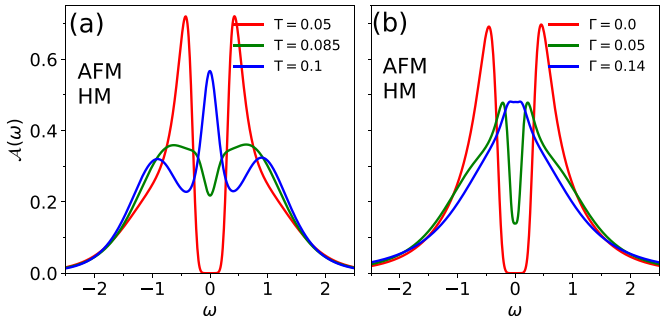

FIG. 4. Comparison of the evolution of the total (i.e., spin averaged) local DOS as a function of T at fixed $\Gamma = 0.0$ (a) and of Γ at fixed $T = 0.01$ (b), at interaction $U = 1.7$, for the AFM-HM across the AFM to PM. The line colors correspond to the spots along the m_s curve of Fig. 2.

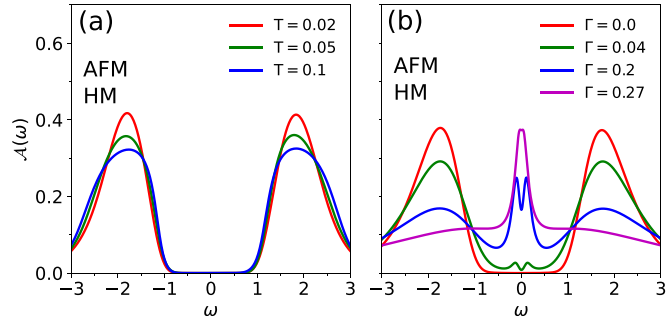

FIG. 5. Comparison of the evolution of the total (i.e., spin averaged) local DOS as a function of T at fixed $\Gamma = 0.0$ (a) and of Γ at fixed $T = 0.01$ (b), at interaction $U = 4.0$, for the AFM-HM across the AFM to PM. The line colors correspond to the spots along the m_s curve of Fig. 2.

with the interaction strength. This means that the reservoir is no longer as effective in suppressing the magnetism.

The physics driving the suppression of m_s with increasing in Γ is qualitatively different from the thermal disorder induced by T. It can be attributed to the Kondo screening of magnetic moment at each site of HM due to the electronic reservoir. This can be most clearly seen if, for a moment, we set the hopping t of the HM to zero, and we obtain a collection of single Anderson impurity models (AIM), at every site. The bath of the AIM is controlled by the strength of Γ. Thus, the local moment of the lattice sites are induced by U, but screened by Γ through the Kondo effect. Therefore, with increasing U, one needs a larger Γ_N to screen m_S and suppress the magnetic order.

To gain a deeper understanding of the observed contrast between similar behaviors of Γ_N and T_N at small U but different at large U, we study the evolution of the local DOS. We have selected specific points across the T- and Γ-driven transitions indicated by the color spots in Fig. 2. The panels (a) and (b) of Fig. 4 display the variation of the local DOS with T and Γ, respectively, for $U = 1.7$. We recall that the DOS looks symmetric because we are showing the total DOS, which is the sum of the up and down spin components, since we are mostly interested in its qualitative evolution. At small T, the HM has AFM order and, consequently, the DOS has a gap at the Fermi energy. As one increases T, m_s decreases, and the gap gradually decreases and fills up. For large enough T, $T \geqslant 0.09$, m_s vanishes and the DOS develops a prominent quasi-particle peak at Fermi energy. This is the familiar Kondo peak that develops in the associated impurity problem [52]. A qualitatively similar behavior is observed in the variation of DOS as one increases Γ while keeping T fixed. However, some quantitative differences are apparent. For instance, the Hubbard sidebands are not so well resolved as the system becomes metallic. This can be understood from the fact that the metallic quasiparticle peak is the manifestation of the Kondo peak in the associated impurity problem. In contrast to the previous $\Gamma = 0$ case, now, the finite value of Γ implies that there is a nonrenormalizable component of the impurity bath, which does not change under the self-consistency condition 7. This "wide" hybridization increases as Γ increases, driving the width of the Kondo peak larger and larger. Hence, the quasiparticle peak is wider, taking significant spectral weight from the Hubbard band components.

In contrast, at large $U = 4.0$, the evolution of the local DOS with increasing T and Γ differs qualitatively from the low U case. The DOS shown in the panel (a) of Fig. 5 hardly changes as T is increased, even though the system undergoes an AFM to PM transition [62,63]. In this case, therefore, instead of an insulator-to-metal transition we have a insulator-to-insulator one. At this large U, the charge degrees of freedom are frozen, which is signaled by the large Mott gap that can be observed. Hence, only the spin degrees of freedom respond to increasing T, which leads to the suppression of the (antiferro)magnetic polarization, but does not affect the charge gap in the DOS, as typical in the Heisenberg regime.

In contrast, the evolution as a function of Γ for low $T = 0.01$ is qualitatively different. We observe that in this case, the local DOS results do reveal an insulator-metal transition. Nevertheless, this transition is also qualitatively different from that of the lower U case. The main feature that emerges in the DOS upon the increase of Γ is the emergence of a two in-gap peak structure around zero frequency, within the Mott-Hubbard band gap. We can understand these two features in terms of the associated impurity problem. Since the state is AF, the spin symmetry is broken into a Néel type of order into two sublattices. Thus, at a given lattice site, the one type of spin has a larger occupation than the opposite, and vice versa on the neighboring site. Thus, one sublattice will have a, say, positive magnetic moment with a higher occupation of the spin-up electrons, while the other sublattice will have the opposite. Thus, each associated impurities, one corresponding at either lattice, will realize a different state. Of course, there is up-down or particle-hole symmetry relating those two states, due to the Néel order.

The crucial point is, nevertheless, that both impurities are in an environment that is not fully gapped as before, but has low-energy states due to the finite Γ. This can be directly seen from the hybridization term associated to Γ in Eq. (8). The consequence for this is that there will be a small Kondo peak emerging near the Fermi energy in the solution of the associated impurity. Since we have two inequivalent impurity sites, one for each sublattice, they lead to the two small quasiparticle peaks that appear in the local DOS in Fig. 5. As we discussed

before, the contribution to the effective bath associated to Γ does not renormalize and remains the same for both spin projections and for both sublattices. As Γ increases we see that the strength of the Kondo peaks increases. Eventually, the screening becomes so strong that the magnetic order collapses as $m_s \to 0$ at Γ_N. At that point, there is a sole quasiparticle peak in the local DOS since the spin symmetry is restored, and the system has gone through an insulator to strongly correlate metal transition.

B. Hubbard and dimer Hubbard models in the paramagnetic state

In previous sections, we have compared the effects of T and Γ on the AFM-PM transition of the HM, which are insulator-to-metal at low U and insulator-to-insulator at large U. We observed that the effects of bath coupling can be considered qualitatively similar at low-interaction U, but become substantially different at large U. We point out that both, the T- and Γ-driven transitions, start out from an insulator state at all U, which is gapped. While this initial study was motivated by the experimental results on the transition in the V_2O_3 heterostructure, it may be interesting to complete the picture to consider the case of the effect of Γ in the well-studied paramagnetic MIT in the Hubbard model as well [52]. In fact, as in this transition the AF order is absent, the system starts in a correlated metal without a gap. So in this section we shall consider the interesting question of whether Γ may also play an analogous role as T does, but this time within paramagnetic states. We shall consider two paradigmatic strongly correlated MIT, that of the HM and the DHM one.

1. Phase diagrams

The MIT in the Hubbard model within the paramagnetic phase is by now a well-known paradigm of a strongly correlated phenomena [52]. The phase diagram in the $T-U$ plane shows a metallic region at low U and low T, a Mott insulator at high U and low T, and a bad metal at higher T in the intermediate U regime. One of the most interesting features is the existence of a coexistence region in between the correlated metal and the Mott insulator, which gives a first-order character to the transition. These well-known results are shown in the phase diagram in panel (a) of Fig. 6. Following a similar strategy as before, we compared the T-driven behavior with that of Γ. The results are shown in the panel (b) of the same figure. We strikingly observe that the behavior of the two parameters is qualitatively similar and the main feature of a triangular coexistence region is preserved. However, there is a qualitative difference, as it can be observed that the tilting of the triangular region has changed.

To gain further insight we turned to the other basic model that we are considering in the present paper, the DHM, which may be relevant, as a first approximation, to the experiments in VO_2 heterostructures. Indeed, the DHM also presents a coexistence region in the $T-U$ phase diagram within the paramagnetic phase [45,46,48]. The phase diagram obtained with CT-QMC simulations is shown in the panel (c) of Fig. 6. We observe in this case that the triangular region is tilted to the right, which is a common feature of cluster DMFT models, and the DHM can be considered as the simplest of those ones [48]. We explored by numerical simulations the fate of the triangular region at the lowest T and increasing Γ. The obtained phase diagram is shown in the panel (d) of the figure. Once again, we observe the feature that the coupling to the electronic reservoir seems to play a similar role as the T, as now even the triangular coexistence region shows a similar tilt.

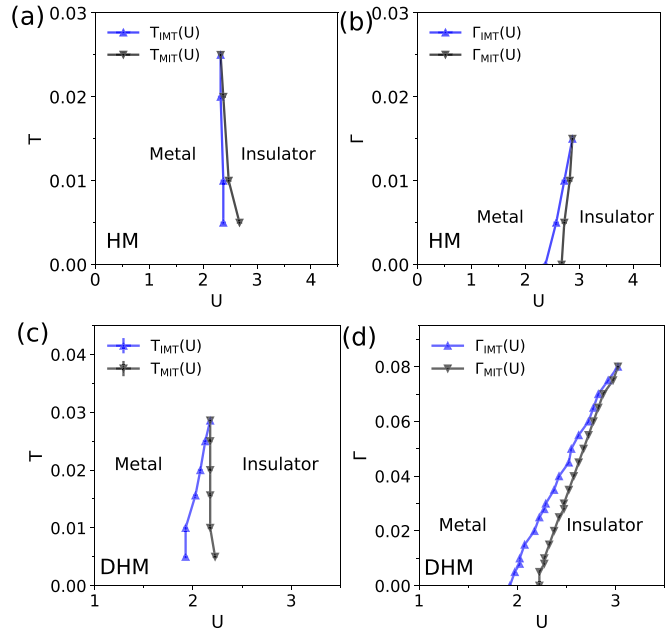

FIG. 6. (a) T-U phase diagram at $\Gamma = 0.0$ (b) Γ-U phase the diagram at $T = 0.01$ of the half-filled HM with PM symmetry. (c) T-U phase diagram at $\Gamma = 0.0$ (d) Γ-U Phase diagram at $T = 0.005$ of the DHM. In the T-U (Γ-U) phase diagram, while increasing U at a given T (Γ), the system goes from metal to insulator at $T_{MIT}(U)$ [$\Gamma_{MIT}(U)$] and while decreasing U system goes from insulator to metal at $T_{IMT}(U)$ [$\Gamma_{IMT}(U)$]. The triangular regions denote the coexistence of solutions, which is consistent with the first-order nature of the experimentally observed transitions.

2. Density of states

To understand further the effect of T and Γ at small U and at large U, we study the systematic changes of DOS for the two models at small and large U. We begin with the results at low U, which are obtained by CT-QMC plus maximal entropy analytic continuation. In Fig. 7 we show the DOS at the small $U = 1.7$ (i.e., metallic side of the transition) for the HM and DHM. Interestingly, we observe that increasing both T and Γ has a qualitatively similar effect in the DOS. They can both control the intensity of the quasiparticle peak; however, increasing T provokes a more significant transfer of weight toward the Hubbard bands with respect to Γ.

We also explore a stronger correlated state for the DHM, namely at $U = 2.2$ within the coexistence region, which is considered relevant for the VO_2 compound [48]. In this case, we start from the insulator state within the coexistence, which as a function of T exhibits a first-order insulator-to-metal transition in qualitative agreement with the mentioned compound. The results for the evolution of the DOS are shown in the panel (e) of Fig. 7, where we observe the metallization

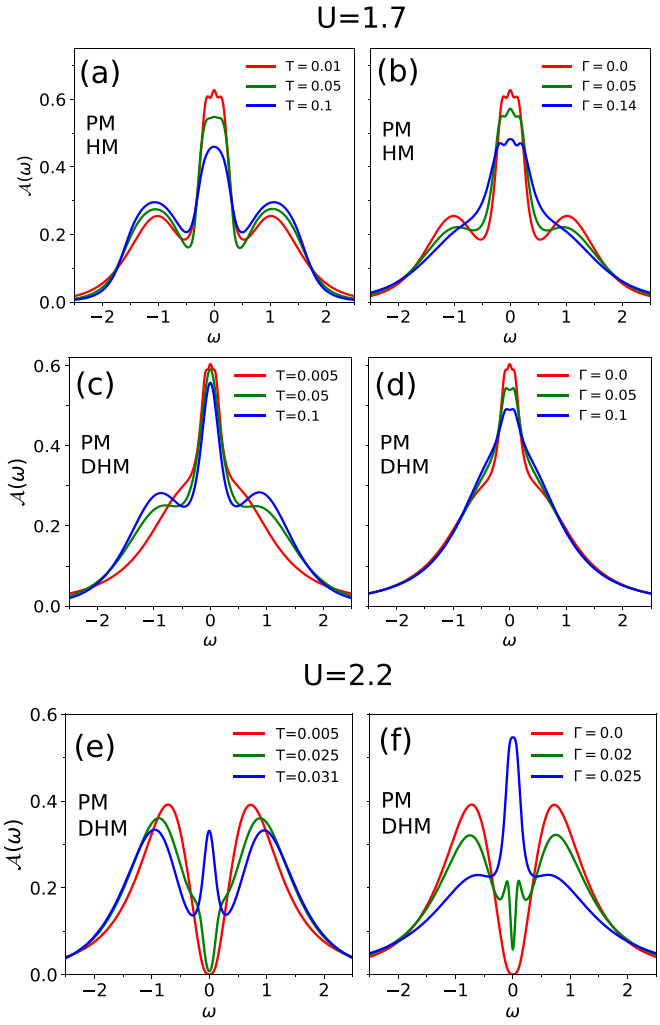

FIG. 7. Side-by-side comparison of the evolution of DOS as a function of T with fixed $\Gamma = 0.0$ [(a), (c), and (e)] and Γ with fixed T [(b), (d), and (f)] in weak interaction region for PM-HM and PM-DHM. (a) (b) and (c) (d) are for PM-HM and PM-DHM at U=1.7, respectively. (e) (f) are for PM-DHM at $U = 2.2$ [64].

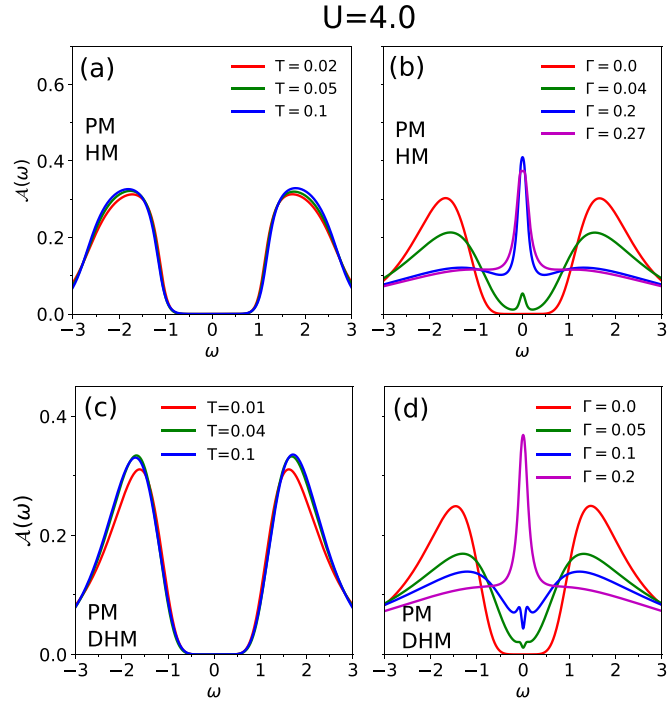

FIG. 8. Side-by-side comparison of the evolution of DOS as a function of T [(a),(c)] and Γ [(b),(d)] at strong interaction $U = 4.0$ for HM and DHM. [(a),(b)] DOS at various T for fixed $\Gamma = 0.0$ and at various Γ for fixed T, respectively, of HM without AFM symmetry. [(c),(d)] DOS of DHM at $U = 4.0$ at various T with fixed $\Gamma = 0.0$ and at various Γ for fixed $T = 0.05$ respectively.

of the correlated insulator. In the panel (f), we report the behavior as a function of Γ for the same starting state. Quite strikingly, we observe a similar behavior. The gap is filled and a prominent quasi-particle peak emerges at the Fermi energy, reminiscent of Kondo physics. Nevertheless, we should also mention that a relatively small difference seems to be present in the evolution of the respective spectra, since at intermediate values of Γ we observe two small quasiparticle peaks at the inner edges of the Hubbard bands, which are not present (or very subtle) in the T-driven case. Another difference is that in the correlated metal state driven by Γ the Hubbard bands have relative smaller spectral intensity as compared to the T-driven transition, which is similar to the effect noted at smaller U.

For completeness, we also considered the large U region, where both systems are deep in the Mott insulator phase. We adopt the relatively large value $U = 4.0$. The results are shown in Fig. 8, where we track changes in the DOS for the two models (HM and DHM) as a function of T and Γ. With increasing temperature at $\Gamma = 0$ on the left-hand side we observe that the DOS hardly changes for both, HM and DHM. Which is natural since the excitation gap at $U = 4$ is much larger than T. However, in striking contrast, the respective DOSs at low T and increasing Γ, shown on the right-hand side of the figure, develop a prominent quasiparticle peak at the Fermi energy.

The interpretation of these behavior also is rooted in the Kondo effect. Indeed, the large value of U create a strong local magnetic model, which at $\Gamma = 0$ is essentially an uncoupled spin, which is a peculiarity of the Mott paramagnet [52]. When the coupling with the electronic bath is switched on, the bath electrons immediately screen the local spins forming Kondo resonances. We may note that a emergence of a Kondo peak in a large Mott gap was reported in systems with a narrow correlated band coupled with a wide conduction band [65] and in the heterostructure of a metal coupled to a Mott insulator [39,40].

Comparing Figs. 7 and 8, and consistent with the Kondo origin of the phenomenon, we observe that the quasiparticle-peak weight increases with Γ at constant U, but decreases with increasing U at constant Γ. At large U, both the HM and the DHM can be driven across an MIT by the intensity of the coupling to the reservoir Γ, but not by T. We may also point out that at large U we also observe in the DOS of the DHM the two small edge quasiparticle peaks that develop as the gap closes.

From the systematic study of the model done so far, with and without magnetic order and at low and large values of U, we observe that there is an emergent pattern. Namely, we can

condense our results noting that to zero order, the effect of T and Γ are qualitatively similar when the interaction U is relatively low. One may be tempted to say that this is in the metallic state and the reason is that the local coupling to the incoherent electron bath plays an analogous role as thermal scattering. This is qualitatively true; however, the argument has even more general validity, since in the AFM *insulator* at low U, both T and Γ also have a qualitatively similar effect. Interestingly, in a recent paper [66] the qualitative difference of the behavior of the AFM Hubbard model at low and large U was investigated. The results showed that in the former case the system is described by a Slater AFM insulator where the bands are splitted by a gap but retain their coherent (i.e., quasiparticle) character. In contrast, at large U the system is a Heisenberg AFM insulator where the (Hubbard) bands are fully incoherent. Hence, in the low U AFM the coupling with the local electron reservoirs disturb the coherent character of the quasi-particle propagation, pretty much as T does.

For completeness, we have constructed a full 3D $T-U-\Gamma$ phase diagram of the HM and DHM where the global behavior in parameter space may be appreciated and is presented in the Supplementary Material.

IV. COMPARISON WITH EXPERIMENTS

We now compare our results with the experimentally observed effect of light illumination on the MIT of vanadate thin films with a deposited layer of photoconductor CDS. The panel (a) of Fig. 9 shows the variation of resistivity (ρ) of CdS/V_2O_3 as a function of T for various values of illumination intensity P (that we qualitatively identify with Γ see Sec. II). The system shows a sharp resistance change across the insulating to metal transition. Significantly, we also note that the transition temperature decreases with increasing illumination intensity. The system's $T_{\rm MIT}$ is driven down to zero temperature for high enough light intensity. We may favorably compare those experimental results with our calculations of the variation of resistivity $\rho(T)$ in the AFM-HM coupled with the electronic reservoir at $U=1.7$ for various values of Γ, that we show in the panel (b) of Fig. 9. For better comparison, we scaled the T with Néel temperature (T_N) at $\Gamma=0$, which is 0.09. The resistivity of our model calculation also shows a sharp decrease of resistivity across MIT, which is associated with the AFM to PM transition. Importantly, one can also note that transition temperature decreases with increasing Γ. Thus, AFM Hubbard model coupled with an electronic reservoir can qualitatively capture the suppression of $T_{\rm MIT}$ observed in CdS/V_2O_3. While the simple one-band Hubbard model may seem a simplistic model of V_2O_3, and in many aspects it is, it is worthy to note that the same model for the same value of the parameter U was adopted to successfully account for nontrivial large negative magnetoresistance effects observed in thin films of the same compound [43].

We now turn to the experiments done on VO_2. The panel (c) of Fig. 9 shows the experimental resistivity of CdS/VO_2 for various values of illumination intensity. The system shows a sharp insulating to metal transition as a function of temperature with sharp resistance change at $T_{\rm MIT}$. Similarly, as before, we scale the T with the $T_{\rm MIT}=308$ K of CdS/VO_2

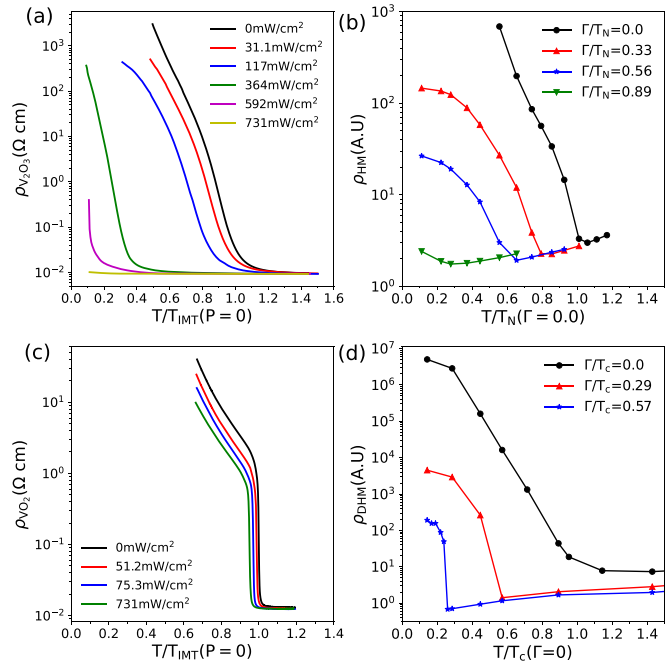

FIG. 9. Comparing temperature-dependent experimental resistivity with theoretically calculated resistivity for various light intensities (P) on CdS/V_2O_3 and CdS/VO_2. (Left) Experimental resistivity (ρ) for CdS/V_2O_3 (top) and CdS/VO_2 (bottom) [17]. (Right) Variation of ρ of HM-AFM at $U=1.7$ (top) and DHM at $U=2.2$ (bottom), as a function of T for various values of Γ. We scale the T with the $T_{\rm MIT}$ of CdS/V_2O_3 with no light on CdS, which is 148 K.

with no light on CdS. Rather surprisingly, there is also a reduction in $T_{\rm MIT}$ upon illumination as seen in CdS/V_2O_3, but the magnitude of the effect for the same light intensity is much less sensitive. We turn to the DHM and set the parameter as were adopted in Refs. [46,48], namely $t_\perp=0.3$ and $U=2.2$ (near the coexistence region) at half-filling ($\mu=U/2$) where that model successfully accounted for some experimentally observed features in VO_2. The panel (d) of Fig. 9 shows the calculated resistivity $\rho(T)$ of the DHM coupled with the electronic reservoir for various values of Γ. For better comparison, we scaled T with the critical temperature $T_c=0.03$ at $\Gamma=0.0$. One can note that transition temperature decreases with increasing Γ as observed for CdS/VO_2 and in the previous case. However, the effect seems too strong as compared to the experimental findings. We have tried varying different parameters in different regions of the phase diagram, but did not find any better agreement.

Since the comparably simple Hubbard model has accounted for V_2O_3 and in view of past success of the DHM model to account for aspects of VO_2, we should try to speculate on the origin of the discrepancy. One natural missing ingredient in the model may be that the structural transition may play a significant role. VO_2 has a larger structural transition that is concurrent with the MIT than V_2O_3, so its relative effect may be more significant [67]. In fact, one may argue that since a structural transition can be understood as due to the condensation of phonon fluctuations, therefore a purely electronic reservoir may not be effective in driving

the system sufficiently. Therefore the effect is still present but in a much smaller magnitude as the MIT is always arrested by the inability of the CdS to promote phononic excitations.

V. CONCLUSIONS

We study the effect of the photoconductor CdS on two strongly correlated vanadate thin films. The theoretical modeling that we introduced consists of a collection of incoherent electronic reservoirs coupled at every lattice site of a Hubbard and a dimer Hubbard model. We note that besides the motivation to account for the experimental observations, these models are also interesting from a fundamental physics point. Indeed, the coupling with electronic reservoirs is a required feature in order to describe electrons on lattices, driven out-of-equilibrium by external electric fields. The currents that develop produce heat that need to be evacuated via reservoirs to allow the system to thermally equilibrate [68].

The coupling strength of those models with the electronic reservoirs is characterized by a parameter Γ, which we argued may play the similar role as the illumination power. These models are solved using DMFT with HYB-CTQMC as an impurity solvers.

From the systematic study we observed that Γ and T played a qualitatively similar role, so long the underlying electronic structure could be described with quasiparticles, which is at low to moderate U, regardless whether the system is a metal or an insulator. We trace that to the fact that the local coupling with the reservoir produces a source of electronic scattering, similarly as the T does.

This observation provided a natural explanation to the dramatic suppression of the transition temperature in V_2O_3, where the insulator state is due to the opening of an antiferromagnetic gap, i.e., of electronic origin. Hence the electronic reservoir was efficient to suppress it. In contrast, the agreement was not so successful for the VO_2 experiments, which show a significant smaller effect of reduction in the transition temperature. We argue that this points to a prominent role of the structural transition, which is couple to lattice vibration degrees of freedom [49], hence the electronic reservoir is less efficient.

It will be interesting in future work to consider the extension of our hybrid model to other strongly correlated models, such as the double exchange model and the periodic Anderson model, which are relevant for other material compounds and may open the way to new forms of control of strongly correlated phenomena.

ACKNOWLEDGMENTS

We acknowledge support from the French ANR MoMA Project No. ANR-19-CE30-0020. L.F. is supported by the Quantum Materials for Energy Efficient Neuromorphic Computing, an Energy Frontier Research Center funded by the US Department of Energy, Office of Science, Basic Energy Sciences under Award No. DE-SC0019273. M.C. is supported by French ANR "Neptun" ANR-19-CE30-0019-01. We thank H. Navarro of UCSD for providing the figure with experimental data and for useful discussions.

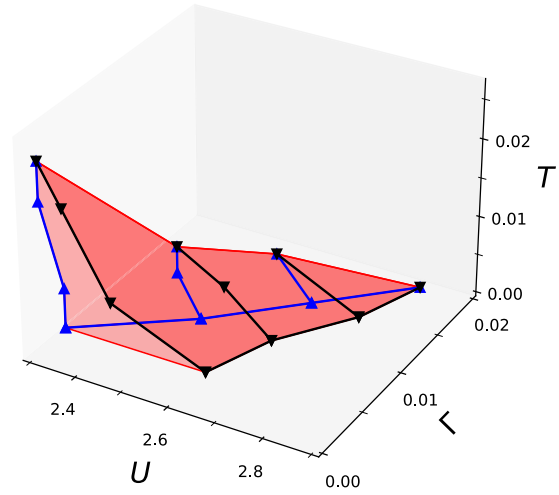

FIG. 10. T-Γ-U phase diagram of HM at half-filling. The coexistence region (colored region) in the $T-U$ plane of the phase diagram shifted toward the right as one increases Γ and T_c decreases with increasing Γ.

APPENDIX A: DC CONDUCTIVITY

The Drude conductivity of HM on Bethe lattice was calculated using

$$\Re\sigma_{\mathrm{HM}}(\omega=0) = 4\int d\epsilon\,\rho(\epsilon)\int d\omega\left(-\frac{\partial f(\omega)}{\partial\omega}\right)_{\omega=0} \times\left(\frac{D^2-\epsilon^2}{3}\right)\left(\mathcal{A}_\uparrow(\epsilon,\omega)\mathcal{A}_\downarrow(\epsilon,\omega) + \mathcal{A}^2_{\mathrm{off}}(\epsilon,\omega)\right) \tag{A1}$$

where $\mathcal{A}_\sigma(\epsilon,\omega)=\frac{-1}{\pi}\mathrm{Im}\frac{z_{\bar\sigma}(\omega)}{z_{\bar\sigma}(\omega)z_\sigma(\omega)-\epsilon^2}$ and $\mathcal{A}_{\mathrm{off}}(\epsilon,\omega)=\frac{-1}{\pi}\mathrm{Im}\frac{\epsilon}{z_{\bar\sigma}(\omega)z_\sigma(\omega)-\epsilon^2}$ with $z_\sigma(\omega)=\omega+\mu-\Sigma_\sigma(\omega)-\Delta_\Gamma(\omega)$.

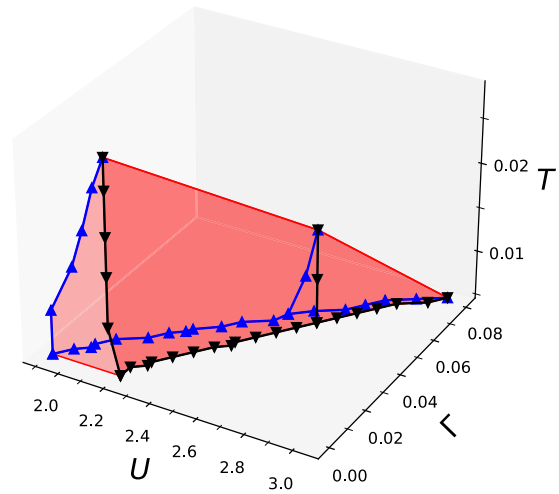

FIG. 11. T-Γ-U phase diagram of DHM at half-filling. The coexistence region (colored region) in the $T-U$ plane of the phase diagram shifted toward the right as one increases Γ and T_c decreases with increasing Γ.

$\frac{D^2-\epsilon^2}{3}$ is the velocity of electron of energy ϵ in Bethe lattice [69].

The DC conductivity of DHM on Bethe lattice was calculated using Eq. [47],

$$\Re\sigma_{\rm DHM}(\omega=0)=2\int d\epsilon\,\rho(\epsilon)\int d\omega\left(-\frac{\partial f(\omega)}{\partial\omega}\right)_{\omega=0}\times\left(\frac{D^2-\epsilon^2}{3}\right)\left(\mathcal{A}^2_{AB}(\epsilon,\omega)+\mathcal{A}^2_{B}(\epsilon,\omega)\right) \tag{A2}$$

where $\mathcal{A}^2_{AB}(\epsilon,\omega)$ and $\mathcal{A}^2_{B}(\epsilon,\omega)$ are DOS of antibond and bond respectively.

APPENDIX B: METAL-INSULATOR COEXISTENCE REGIONS

We display here the metal-insulator coexistence region in the full $T-U-\Gamma$ phase diagram. Notice the difference in the tilting between the Hubbard (HM) (Fig. 10) and Dimer Hubbard (DHM) (Fig. 11) models by cutting $T-U$ planes.

[1] J. Del Valle, J. G. Ramírez, M. J. Rozenberg, and I. K. Schuller, Challenges in materials, and devices for resistive-switching-based neuromorphic computing, J. Appl. Phys. **124**, 211101 (2018).

[2] P. Stoliar, J. Tranchant, B. Corraze, E. Janod, M.-P. Besland, F. Tesler, M. Rozenberg, and L. Cario, A leaky-integrate-and-fire neuron analog realized with a Mott insulator, Adv. Funct. Mater. **27**, 1604740 (2017).

[3] M. D. Pickett, G. Medeiros-Ribeiro, and R. S. Williams, A scalable neuristor built with Mott memristors, Nat. Mater. **12**, 114 (2013).

[4] R. Luo, X. Zhao, L. Chen, T. J. Legvold, H. Navarro, I. K. Schuller, and D. Natelson, Spin Seebeck effect at low temperatures in the nominally paramagnetic insulating state of vanadium dioxide, Appl. Phys. Lett. **121**, 102404 (2022).

[5] E. Qiu, P. Salev, L. Fratino, R. Rocco, H. Navarro, C. Adda, J. Li, M.-H. Lee, Y. Kalcheim, M. Rozenberg, and I. K. Schuller, Stochasticity in the synchronization of strongly coupled spiking oscillators, Appl. Phys. Lett. **122**, 094105 (2023).

[6] S. Cheng, M.-H. Lee, R. Tran, Y. Shi, X. Li, H. Navarro, C. Adda, Q. Meng, L.-Q. Chen, R. C Dynes *et al.*, Inherent stochasticity during insulator–metal transition in VO_2, Proc. Natl. Acad. Sci. USA **118**, e2105895118 (2021).

[7] S. Kumar, M. D. Pickett, J. P. Strachan, G. Gibson, Y. Nishi, and R. S. Williams, Local temperature redistribution, and structural transition during Joule-heating-driven conductance switching in VO_2, Adv. Mater. **25**, 6128 (2013).

[8] S. Chen, Z. Wang, L. Fan, Y. Chen, H. Ren, H. Ji, D. Natelson, Y. Huang, J. Jiang, and C. Zou, Sequential insulator-metal-insulator phase transitions of VO_2 triggered by hydrogen doping, Phys. Rev. B **96**, 125130 (2017).

[9] M. Yang, Y. Yang, B. Hong, L. Wang, K. Hu, Y. Dong, H. Xu, H. Huang, J. Zhao, H. Chen *et al.*, Suppression of structural phase transition in VO_2 by epitaxial strain in vicinity of metal-insulator transition, Sci. Rep. **6**, 1 (2016).

[10] D. G. Schlom, L.-Q. Chen, C. J. Fennie, V. Gopalan, D. A. Muller, X. Pan, R. Ramesh, and R. Uecker, Elastic strain engineering of ferroic oxides, MRS Bull. **39**, 118 (2014).

[11] N. B. Aetukuri, A. X. Gray, M. Drouard, M. Cossale, L. Gao, A. H. Reid, R. Kukreja, H. Ohldag, C. A. Jenkins, E. Arenholz *et al.*, Control of the metal–insulator transition in vanadium dioxide by modifying orbital occupancy, Nat. Phys. **9**, 661 (2013).

[12] Y. H. Matsuda, D. Nakamura, A. Ikeda, S. Takeyama, Y. Suga, H. Nakahara, and Y. Muraoka, Magnetic-field-induced insulator–metal transition in W-doped VO_2 at 500 T, Nat. Commun. **11**, 3591 (2020).

[13] B. Wu, A. Zimmers, H. Aubin, R. Ghosh, Y. Liu, and R. Lopez, Electric-field-driven phase transition in vanadium dioxide, Phys. Rev. B **84**, 241410(R) (2011).

[14] J. Jeong, N. Aetukuri, T. Graf, T. D. Schladt, M. G. Samant, and S. S. P Parkin, Suppression of metal-insulator transition in VO_2 by electric field–induced oxygen vacancy formation, Science **339**, 1402 (2013).

[15] C. Wan, E. H. Horak, J. King, J. Salman, Z. Zhang, Y. Zhou, P. Roney, B. Gundlach, S. Ramanathan, R. H. Goldsmith *et al.*, Limiting optical diodes enabled by the phase transition of vanadium dioxide, ACS Photon. **5**, 2688 (2018).

[16] K. Dong, S. Hong, Y. Deng, H. Ma, J. Li, X. Wang, J. Yeo, L. Wang, S. Lou, K. B. Tom *et al.*, A lithography-free, and field-programmable photonic metacanvas, Adv. Mater. **30**, 1703878 (2018).

[17] H. Navarro, J. del Valle, Y. Kalcheim, N. M. Vargas, C. Adda, M.-H. Lee, P. Lapa, A. Rivera-Calzada, I. A Zaluzhnyy, E. Qiu *et al.*, A hybrid optoelectronic Mott insulator, Appl. Phys. Lett. **118**, 141901 (2021).

[18] Y. Ke, S. Wang, G. Liu, M. Li, T. J. White, and Y. Long, Vanadium dioxide: The multistimuli responsive material, and its applications, Small **14**, 1802025 (2018).

[19] A. Singer, J. G. Ramirez, I. Valmianski, D. Cela, N. Hua, R. Kukreja, J. Wingert, O. Kovalchuk, J. M. Glownia, M. Sikorski, M. Chollet, M. Holt, I. K. Schuller, and O. G. Shpyrko, Nonequilibrium phase precursors during a photoexcited insulator-to-metal transition in V_2O_3, Phys. Rev. Lett. **120**, 207601 (2018).

[20] H. Navarro, A. C. Basaran, F. Ajejas, L. Fratino, S. Bag, T. D. Wang, E. Qiu, V. Rouco, I. Tenreiro, F. Torres, A. Rivera-Calzada, J. Santamaria, M. Rozenberg, and I. K. Schuller, Light-induced decoupling of electronic, and magnetic properties in manganites, Phys. Rev. Appl. **19**, 044077 (2023).

[21] C. Adda, H. Navarro, J. Kaur, M.-H. Lee, C. Chen, M. Rozenberg, S. P Ong, and I. K. Schuller, An optoelectronic heterostructure for neuromorphic computing: CdS/V_3O_5, Appl. Phys. Lett. **121**, 041901 (2022).

[22] J. A Aman, Brian J. DeSalvo, F. B Dunning, T. C Killian, S. Yoshida, and J. Burgdörfer, Trap losses induced by near-resonant Rydberg dressing of cold atomic gases, Phys. Rev. A **93**, 043425 (2016).

[23] J. Zeiher, R. Van Bijnen, P. Schauß, S. Hild, J.-y. Choi, T. Pohl, I. Bloch, and C. Gross, Many-body interferometry

of a Rydberg-dressed spin lattice, Nat. Phys. **12**, 1095 (2016).
[24] B. Kraus, H. P. Büchler, S. Diehl, A. Kantian, A. Micheli, and P. Zoller, Preparation of entangled states by quantum Markov processes, Phys. Rev. A **78**, 042307 (2008).
[25] J. Kaczmarczyk, H. Weimer, and M. Lemeshko, Dissipative preparation of antiferromagnetic order in the Fermi-Hubbard model, New J. Phys. **18**, 093042 (2016).
[26] S. Diehl, A. Micheli, A. Kantian, B. Kraus, HP Büchler, and P. Zoller, Quantum states, and phases in driven open quantum systems with cold atoms, Nat. Phys. **4**, 878 (2008).
[27] A. Amaricci, C. Weber, M. Capone, and G. Kotliar, Approach to a stationary state in a driven Hubbard model coupled to a thermostat, Phys. Rev. B **86**, 085110 (2012).
[28] J. Li, C. Aron, G. Kotliar, and J. E. Han, Electric-field-driven resistive switching in the dissipative Hubbard model, Phys. Rev. Lett. **114**, 226403 (2015).
[29] J. del Valle, N. M. Vargas, R. Rocco, P. Salev, Y. Kalcheim, P. N. Lapa, C. Adda, M.-H. Lee, P. Y. Wang, L. Fratino *et al.*, Spatiotemporal characterization of the field-induced insulator-to-metal transition, Science **373**, 907 (2021).
[30] J. del Valle, P. Salev, F. Tesler, N. M. Vargas, Y. Kalcheim, P. Wang, J. Trastoy, M.-H. Lee, G. Kassabian, J. G. Ramírez *et al.*, Subthreshold firing in Mott nanodevices, Nature (London) **569**, 388 (2019).
[31] P. Diener, E. Janod, B. Corraze, M. Querré, C. Adda, M. Guilloux-Viry, S. Cordier, A. Camjayi, M. Rozenberg, M. P. Besland, and L. Cairo, How a dc electric field drives Mott insulators out of equilibrium, Phys. Rev. Lett. **121**, 016601 (2018).
[32] R. Rocco, J. del Valle, H. Navarro, P. Salev, I. K. Schuller, and M. Rozenberg, Exponential escape rate of filamentary incubation in Mott spiking neurons, Phys. Rev. Appl. **17**, 024028 (2022).
[33] S. Thiel, G. Hammerl, A. Schmehl, C. W. Schneider, and J. Mannhart, Tunable quasi-two-dimensional electron gases in oxide heterostructures, Science **313**, 1942 (2006).
[34] A. Euverte, F. Hébert, S. Chiesa, R. T. Scalettar, and G. G. Batrouni, Kondo screening, and magnetism at interfaces, Phys. Rev. Lett. **108**, 246401 (2012).
[35] M. Jiang, G. G. Batrouni, and R. T. Scalettar, Density of states, and magnetic correlations at a metal-Mott insulator interface, Phys. Rev. B **86**, 195117 (2012).
[36] W. Hu, R. T. Scalettar, E. W. Huang, and B. Moritz, Effects of an additional conduction band on the singlet-antiferromagnet competition in the periodic, Anderson model, Phys. Rev. B **95**, 235122 (2017).
[37] S. Sen and N. S. Vidhyadhiraja, Quantum critical Mott transitions in a bilayer Kondo insulator-metal model system, Phys. Rev. B **93**, 155136 (2016).
[38] R. Peters, Y. Tada, and N. Kawakami, Kondo effect in f-electron superlattices, Phys. Rev. B **88**, 155134 (2013).
[39] R. W. Helmes, T. A. Costi, and A. Rosch, Kondo proximity effect: How does a metal penetrate into a Mott insulator? Phys. Rev. Lett. **101**, 066802 (2008).
[40] G. Borghi, M. Fabrizio, and E. Tosatti, Strongly correlated metal interfaces in the Gutzwiller approximation, Phys. Rev. B **81**, 115134 (2010).
[41] H. Zenia, J. K Freericks, H. R Krishnamurthy, and T. Pruschke, Appearance of fragile Fermi liquids in finite-width Mott insulators sandwiched between metallic leads, Phys. Rev. Lett. **103**, 116402 (2009).
[42] M. Imada, A. Fujimori, and Y. Tokura, Metal-insulator transitions, Rev. Mod. Phys. **70**, 1039 (1998).
[43] J. Trastoy, A. Camjayi, J. del Valle, Y. Kalcheim, J.-P. Crocombette, D. A. Gilbert, J. A. Borchers, J. E. Villegas, D. Ravelosona, M. J. Rozenberg, and I. K. Schuller, Magnetic field frustration of the metal-insulator transition in V_2O_3, Phys. Rev. B **101**, 245109 (2020).
[44] S. Biermann, A. Poteryaev, A. I. Lichtenstein, and A. Georges, Dynamical singlets, and correlation-assisted Peierls transition in VO_2, Phys. Rev. Lett. **94**, 026404 (2005).
[45] O. Nájera, M. Civelli, V. Dobrosavljević, and M. J. Rozenberg, Multiple crossovers, and coherent states in a Mott-Peierls insulator, Phys. Rev. B **97**, 045108 (2018).
[46] H. T Stinson, A. Sternbach, O. Najera, R. Jing, A. S Mcleod, T. V Slusar, A. Mueller, L. Anderegg, H. T Kim, M. Rozenberg *et al.*, Imaging the nanoscale phase separation in vanadium dioxide thin films at terahertz frequencies, Nat. Commun. **9**, 3604 (2018).
[47] O. N. Ocampo, Study of the dimer Hubbard model within dynamical mean field theory, and its application to VO_2, Ph.D. thesis, Université Paris, Saclay, 2017.
[48] O. Nájera, M. Civelli, V. Dobrosavljević, and M. J. Rozenberg, Resolving the VO_2 controversy: Mott mechanism dominates the insulator-to-metal transition, Phys. Rev. B **95**, 035113 (2017).
[49] F. Grandi, A. Amaricci, and M. Fabrizio, Unraveling the Mott-Peierls intrigue in vanadium dioxide, Phys. Rev. Res. **2**, 013298 (2020).
[50] K. Deng and L. Li, CdS nanoscale photodetectors, Adv. Mater. **26**, 2619 (2014).
[51] L. Cheng, Q. Xiang, Y. Liao, and H. Zhang, CdS-based photocatalysts, Energ. Environ. Sci. **11**, 1362 (2018).
[52] A. Georges, G. Kotliar, W. Krauth, and M. J. Rozenberg, Dynamical mean-field theory of strongly correlated fermion systems, and the limit of infinite dimensions, Rev. Mod. Phys. **68**, 13 (1996).
[53] G. A. Boiko V. S. Dneprovskii, M. V. Kraevskii, K. Marinova, S. M. Oak, E. K. Silina, and V. S. Fokin, A study of the kinetics of recombination radiation of CdS, and CdSe crystals, Phys. Stat. Sol. (B) **85**, 111 (1978).
[54] E. Gull, A. J. Millis, A. I. Lichtenstein, A. N. Rubtsov, M. Troyer, and P. Werner, Continuous-time Monte Carlo methods for quantum impurity models, Rev. Mod. Phys. **83**, 349 (2011).
[55] P. Werner and A. J. Millis, Hybridization expansion impurity solver: General formulation, and application to Kondo lattice, and two-orbital models, Phys. Rev. B **74**, 155107 (2006).
[56] K. Haule, Quantum Monte Carlo impurity solver for cluster dynamical mean-field theory, and electronic structure calculations with adjustable cluster base, Phys. Rev. B **75**, 155113 (2007).
[57] G. Moeller, V. Dobrosavljević, and A. E. Ruckenstein, RKKY interactions and the Mott transition, Phys. Rev. B **59**, 6846 (1999).
[58] L. Fratino, S. Bag, A. Camjayi, M. Civelli, and M. Rozenberg, Doping-driven resistive collapse of the Mott insulator in a minimal model for VO_2, Phys. Rev. B **105**, 125140 (2022).
[59] M. Jarrell and J. E. Gubernatis, Bayesian inference, and the analytic continuation of imaginary-time quantum Monte Carlo data, Phys. Rep. **269**, 133 (1996).

[60] S. Bag, A. Garg, and H. R. Krishnamurthy, Phase diagram of the half-filled ionic Hubbard model, Phys. Rev. B **91**, 235108 (2015).

[61] L. Fratino, P. Sémon, M. Charlebois, G. Sordi, and A.-M. S. Tremblay, Signatures of the Mott transition in the antiferromagnetic state of the two-dimensional Hubbard model, Phys. Rev. B **95**, 235109 (2017).

[62] M. J. Rozenberg, G. Kotliar, H. Kajueter, G. A. Thomas, D. H. Rapkine, J. M. Honig, and P. Metcalf, Optical conductivity in Mott-Hubbard systems, Phys. Rev. Lett. **75**, 105 (1995).

[63] A. Camjayi, R. Chitra, and M. J. Rozenberg, Electronic state of a doped Mott-Hubbard insulator at finite temperatures studied using the dynamical mean-field theory, Phys. Rev. B **73**, 041103(R) (2006).

[64] The MaxEnt formalism tends to produce spurious noise around the ω=0 point. this is usually not problematic for insulating solutions, but not desirable for metallic spectral functions. J. Skilling, Fundamentals of MaxEnt in data analysis, in *Maximum Entropy in Action*, edited by B. Buck and V. A. Macaulay (Clarendon Press, Oxford, 1991), p. 19, https://triqs.github.io/maxent/latest/guide/preblur.html.

[65] L. de' Medici, A. Georges, G. Kotliar, and S. Biermann, Mott transition, and Kondo screening in f-electron metals, Phys. Rev. Lett. **95**, 066402 (2005).

[66] P. Foulquier, M. Civelli, M. Rozenberg, A. Camjayi, J. Bobadilla, D. Colson, A. Forget, P. Thuéry, F. Bertran, P. L. Févre, and V. Brouet, Evolution of the spectral lineshape at the magnetic transition in Sr_2IrO_4, and Sr_3Ir_2 O_7, Eur. Phys. J. B **96**, 42 (2023).

[67] J. D. Budai, J. Hong, M. E. Manley, E. D. Specht, C. W. Li, J. Z. Tischler, D. L. Abernathy, A. H. Said, B. M. Leu, L. A. Boatner *et al.*, Metallization of vanadium dioxide driven by large phonon entropy, Nature (London) **515**, 535 (2014).

[68] M. I. Díaz, J. E. Han, and C. Aron, Electrically driven insulator-to-metal transition in a correlated insulator: Electronic mechanism, and thermal description, Phys. Rev. B **107**, 195148 (2023).

[69] W. Chung and J. K. Freericks, Charge-transfer metal-insulator transitions in the spin-$\frac{1}{2}$ Falicov-Kimball model, Phys. Rev. B **57**, 11955 (1998).